Design and Implementation of High-Misalignment Tolerance WPT System for Underwater Vehicles Based on a Variable Inductor

Jia Li, Chong Zhu, *Member, IEEE*, Jixie Xie, Fei Lu, *Member, IEEE*, and Xi Zhang, *Senior Member, IEEE*

***Abstract*— Wireless charging for autonomous underwater vehicles has been widely explored recently by the merit of safety and convenience. However, due to the misalignment between charging coils in the horizontal and vertical directions, the system may not maintain constant current or constant voltage output. Therefore, this article proposes a mistuned inductive power transfer (IPT) system structure and corresponding design methods to improve misalignment tolerance. The proposed IPT system adopts series–series compensation and includes a variable inductor (VI) on the secondary side. A general design method based on the established mathematical model is proposed. The worst scenarios (i.e., the maximum value of misalignment) are used for the optimization of the system parameters. The control strategy for VI without any communication link to the primary side is established. Finally, a 1-kW IPT system for tolerance of k of 0.15–0.5 and output voltage of 74–150 V variation is set up. The experimental results show that the horizontal and vertical direction misalignment ranges reach $\pm 47\%$ and $+140\%$, respectively, and the maximum system efficiency exceeds 96% for full power output. The proposed system improves the freedom and stability of charging in the harsh underwater environment.**

***Index Terms*—Constant current (CC), inductive power transfer (IPT), misalignment tolerance, variable inductor (VI).**

I. Introduction

INDUCTIVE power transfer (IPT) technique has been widely applied in various applications, such as portable electronic products, electric vehicles, and underwater devices [1], [2], [3]. Compared to conventional plug-in charging systems, IPT offers numerous advantages in relation to electrical isolation, safety, flexibility, and convenience.

For underwater IPT systems, one of the main challenges is to eliminate the adverse effects [4] caused by misalignment between the transmitter and receiver while maintaining the load-independent characteristics. Especially for underwater environment, the turbulent water condition makes it difficult for strict alignment between the primary and secondary coils. In addition, apart from the commonly considered horizontal misalignment in on land IPT systems, vertical misalignment becomes significant in underwater IPT systems. Another challenge is the high attenuation provided by seawater to high-frequency signals. Establishing a stable communication with low latency and bit error rate is challenging in underwater environment.

Several research has been carried out to deal with the problem. The methods can be separated into three categories that can be termed as "magnetic coupler structure design" [5], [6], [7], [11], "compensation topology design" [12], [13], [14], [15], [16], [17], [18], [19], [20], and "active control strategy" [21], [22], [23], [24], [25], [26], [27], [28], [29], [30], [31], [32], [33], [34]. First, the magnetic coupler structure can be designed to seek a relatively stable equivalent mutual inductance when misalignment occurs. For example, coaxial ring-shaped [5], quadruple-coil shaped [6], rotation-free shaped [7], [8], and three-phase ring shaped couplers [9] have been proposed for underwater IPT systems. Based on the previous articles, the proposed magnetic couplers can improve the feasibility for underwater environment. Whereas, most magnetic coupler structures have only single direction improvement for misalignment tolerance [e.g., the rotation-free WPT system for autonomous underwater vehicle (AUV) [7], which improves the performance during the rotational misalignments]. Accordingly, a new magnetic coupler design method has been proposed based on planar couplers. The transmitter coils are designed as two parts, which are connected reversely. Thus, the variations of the mutual inductances among the transmitter and receiver coils can be opposite with misalignment, resulting in a relatively stable equivalent mutual inductance. In [10], a third coil is reversely connected in series with the primary coil, the proposed *LCT*-TC can improve the misalignment performance in x- and y-directions with the inherent output characteristic of double-sided *LCC* topology. However, since the decline in mutual inductances should be the same with misalignment, the coil design freedom is constrained. And the design method may decrease the effective magnetic field for power transfer. In [11], an integrated design for *LCC*-S topology is proposed. The compensation coil is also designed

Manuscript received 30 November 2022; revised 14 February 2023; accepted 30 March 2023. Date of publication 14 April 2023; date of current version 1 September 2023. This work was supported by the National Natural Science Foundation of China under Grant 52007119. *(Corresponding author: Chong Zhu.)*

Jia Li, Chong Zhu, Jixie Xie, and Xi Zhang are with the School of Mechanical Engineering, Shanghai Jiao Tong University, Shanghai 200240, China. (e-mail: 18852647159@sjtu.edu.cn; chong.zhu@sjtu.edu.cn; xiejixie@sjtu.edu.cn; braver1980@sjtu.edu.cn).

Fei Lu is with the Department of Electrical and Computer Engineering, Drexel University, Philadelphia, PA 19104 USA. (e-mail: fei.lu@drexel.edu).

Color versions of one or more figures in this article are available at https://doi.org/10.1109/TPEL.2023.3267104.

Digital Object Identifier 10.1109/TPEL.2023.3267104

as a reversed-series structure. A higher degree of freedom in the coil design is achieved by adjusting a stability factor. In [12], a reversely connected inner coil is used to stabilize the system output under horizontal misalignment conditions. And a finite-element-analysis-based coil optimization algorithm is proposed, which is time consuming.

The second option to deal with the misalignment is concerned to compensation topologies design. Since the output characteristics for various topologies may differ [13]. In [14], a misalignment-tolerant S-SP compensation topology is designed with constant current (CC) or voltage (CV) output characteristics. Furthermore, hybrid compensation topology is proposed to extend the misalignment range. In [15], a hybrid compensation topology with S-*LCC* and *LCC*-S is employed to ensure a stable output current for both load and coupling variations. D-*LCC* and S-S hybrid topologies are also proposed in [16], [17], and [18], with two resonant networks connected in parallel or series. The problem with hybrid topology is the use of too many passive components, causing extra loss and design complexity. In addition, various high-order compensation topologies with optimized parameters are proposed to improve the misalignment tolerance, such as S-SP [19] and *LCC*-SP [20], which can provide a capability of misalignment tolerance for the coupling coefficient by optimization of parameters. In [21], the parameter design for *LCC*-S and double-sided *LCC* topology are analyzed to reduce the misalignment effect. However, these approaches have no constant output characteristics with varied load, which is vital for IPT systems.

The third option for the anti-misalignment of IPT is to employ an active control system that can maintain constant output under misalignments. The methods are mainly applied in IPT systems on land, and a communication link is often necessary for data transfer. Various control methods, such as phase-shift modulation of full-bridge converters [22], [23] and various frequencies [24], have been proposed to maintain stable output versus load and coupling variation. Primary or secondary dc–dc converters are also applied to regulate the output power by adjusting the input voltage or equivalent load for efficiency optimization [25], [26]. However, the use of an extra dc–dc converter may cause power loss, degrading the overall efficiency of the system. Therefore, a dual-side controlled IPT system with an active rectifier is proposed [27], [28], [29]. Two controllers are required to control the output rectifier pulsewidth and input inverter pulsewidth, respectively, to achieve high efficiency over a wide operating range. The drawback of the method is the absence of load-independent characteristics and use of wireless communication link. In [30], a primary control method for CC and CV charging according to the principle of fractional-order autonomous circuit is designed, the proposed system can maintain stable output under misalignment of coupling coils and load variation. Nevertheless, the phase detection requirement may increase the system's complexity. Apart from control of primary and secondary converters, different dynamic tuning methods are proposed with variable capacitor (VC) [31] or variable inductor (VI) [32]. In [33], VC and VI are applied in the primary side of a D-*LCC* compensation topology to improve the misalignment tolerance. Although there is no wireless communication link to exchange information between the primary and secondary sides, it may not be suitable for underwater IPT due to the nonnegligible vertical misalignment and load variation during operation. In [34], a reconfigurable rectifier-based IPT system is proposed for anti-misalignment. However, the fluctuation of the output is inevitable.

Considering the previous article, existing research on anti-misalignment in all directions with load-independent output for underwater IPT is insufficient. For the magnetic coupler and compensation topology optimization, the structure and parameter design may be difficult for all direction misalignment tolerance because of the limitation in design freedom. For the active control methods, a wireless communication link and relatively complex control strategy are often necessary to implement the proposed control scheme, which is not suitable for underwater environment due to the high attenuation provided by seawater to high-frequency signals.

To solve the above problem, this article attempts to design a mistuned IPT system using a VI to regulate the output current to achieve CC output within a wide range of misalignment in both horizontal and vertical directions and load variation. Wireless communication is avoided here.

Without loss of generality, an S-S compensation topology with planar square coils is applied to implement the design. As a widely used compensation topology, S-S features a simple structure with the least passive components and independent compensation from coupling and load. The contributions of this article are as follows:

1) A detuned S-S compensation topology with a secondary VI IPT system is established to achieve both load-independent and misalignment tolerant CC output without any wireless communication link required in most control strategies.
2) A general principle for optimization of parameters of the system is established to guarantee the ZVS condition for CC output with misalignment and load variation. The voltage stress and range of VI are minimized.
3) Compared with previous control strategies, a much simpler control strategy is employed to realize the regulation of output current during misalignment. The communication link between the transmitter and receiver is not necessary in the procedure.
4) An improved misalignment tolerance, especially for vertical misalignment is guaranteed. When the gap ranges from 50 to 120 mm, the proposed system could remain CC output, and the efficiency exceeds 87% with the worst scenario.

II. Theoretical Analysis

A. S-S System Performance Under Misalignment

The proposed system scheme is shown in Fig. 1. An H-bridge inverter converts the primary dc voltage U_{bus} to 85 kHz ac voltage U_{AB}. U_{ab} represents the receiver ac voltage. L_p and L_s are self-inductances and parasitic resistances of the coupling coils. C_p and C_s are compensated capacitors, and M_1 is the mutual inductance between L_p and L_s. The battery can be modeled as a

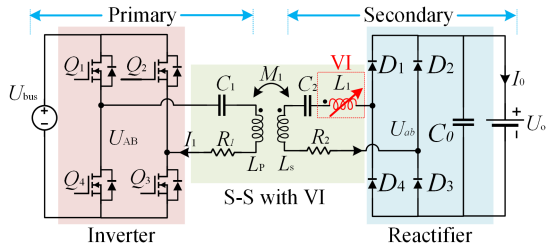

Fig. 1. Structure of the proposed SS-IPT system with VI.

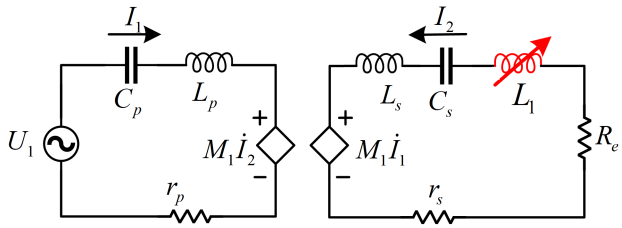

Fig. 2. Mutual inductance model for the proposed topology.

resistor R_0. I_1 and I_2 denote the transmitter and receiver currents. Compared with the traditional S-S system, a VI is introduced on the secondary side to control the output current.

Neglecting the parasitic resistances of the coupling coils, the primary and secondary currents of a conventional S-S system are

$$I_1 = \frac{U_{ab}}{\omega M_1} \tag{1}$$

$$I_2 = \frac{U_{AB}}{\omega M_1} \tag{2}$$

where ω denotes the resonant angular frequency.

From (1) and (2), if the mutual inductance varies as misalignment happens, the system cannot maintain a stable condition any more, and the output current will be much higher than the rated value, inducing a risk of overcurrent.

Therefore, if no additional control is introduced, the resonant S-S IPT system cannot keep CC output with variation of coupling coefficient. To deal with it, detuned compensation topologies are proposed [20] to transfer a relatively constant power over misalignment. However, the load-independent output characteristics will be lost because of the detuned effects. Then, VI and VC are proposed to adjust the degree of detuning for efficiency optimization and ZVS. Compared with VI, the VC method requires a much more complicated strategy to reach the equivalent capacitor value. And the extra VI or VC may always be applied on the primary side, then a wireless communication link is necessary for control, increasing the cost of the whole system. Especially in the underwater environment, wireless communication may be. Therefore, a mistuned SS-IPT system with VI on the secondary side is proposed.

B. System Structure

With a VI introduced on the secondary side, the characteristics of the proposed system should be discussed first. Here, some assumptions are made for analysis as follows: 1) all the internal resistances of passive components are neglected to simplify the analysis; 2) the classical fundamental harmonic approximation method is still accurate enough despite the detuning condition of the compensation topology; and 3) the rectifier part is modeled as an equivalent resistor R_e. The equivalent mutual inductance model is shown in Fig. 2.

According to KVL, the signals in the transmitter and receiver should satisfy

$$\begin{cases} U_1 = \left(j\omega L_p + \frac{1}{j\omega C_p}\right) I_1 + j\omega M_1 I_2 \\ 0 = j\omega M_1 I_1 + \left(j\omega L_s + \frac{1}{j\omega C_s} + j\omega L_1\right) I_2 + R_e I_2 \end{cases} \tag{3}$$

where j is the imaginary unit and R_e represents the equivalent load resistance of the rectifier part, and can be regarded as

$$R_e = \frac{8}{\pi^2} R_0. \tag{4}$$

Here, the sum impedance of L_p and C_p is jX_1; and the sum impedance of L_s, C_s, and L_1 is jX_2, as follows:

$$jX_1 = j\omega L_p + \frac{1}{j\omega C_p} \tag{5}$$

$$jX_2 = j\omega L_s + \frac{1}{j\omega C_s} + j\omega L_1. \tag{6}$$

Expression of I_1 and I_2 are deduced

$$I_1 = \frac{U_1}{jX_1 + \frac{\omega^2 k^2 L^2}{jX_2 + R_e}} = \frac{U_1}{\frac{\omega^2 k^2 L^2 R_e}{R_e^2 + X_2^2} + j\left(X_1 - X_2 \frac{\omega^2 k^2 L^2}{R_e^2 + X_2^2}\right)} \tag{7}$$

$$I_2 = \frac{U_1}{j\omega kL - \frac{jX_1(jX_2 + R_e)}{j\omega kL}} = \frac{U_1}{\frac{-X_1 R_e}{\omega kL} + j\left(\omega kL - \frac{X_1 X_2}{\omega kL}\right)}. \tag{8}$$

The root-mean-square (rms) value of I_2 can be deduced from (8) as

$$|I_2| = \frac{V_1}{\sqrt{\omega^2 k^2 L^2 + \frac{X_1^2(R_e^2 + X_2^2)}{\omega^2 k^2 L^2} - 2X_1 X_2}} \tag{9}$$

where V_1 is the rms value of U_1, $L = \sqrt{L_p L_s}$.

The output current I_2 versus the coupling coefficient k under different X_1 and X_2 is plotted in Fig. 3. From Fig. 3(a), if the primary resonant tank is detuned ($X_1 \neq 0$) and the value of X_1 and R_0 is fixed, I_2 can keep almost constant over a certain range of misalignment. As shown in the picture, the rated current is I_0 (Line A-C). With an allowable variation of 5%, the output current can be regarded as stable for $k = 0.22-0.37$ when $X_2/\omega L$ equals 3.65%. Further, the system can still maintain the desired out current in a weaker ($k = 0.15-0.22$) and stronger ($k = 0.37-0.5$) coupling condition with a variable X_2 (-12.2% to 3.65%). Track of point A to C just proves that.

Similarly, from Fig. 3(b), with the coupling coefficient k being 0.2 and X_1 being 27 Ω, a constant output current (7.07 A) is achieved by adjusting the value of X_2. Track of point D to E prove the feasibility of this control strategy for load-independent output characteristics.

The above features provide an attractive idea for the improvement of the system's misalignment tolerance and load-independent characteristics. However, in order for a relatively

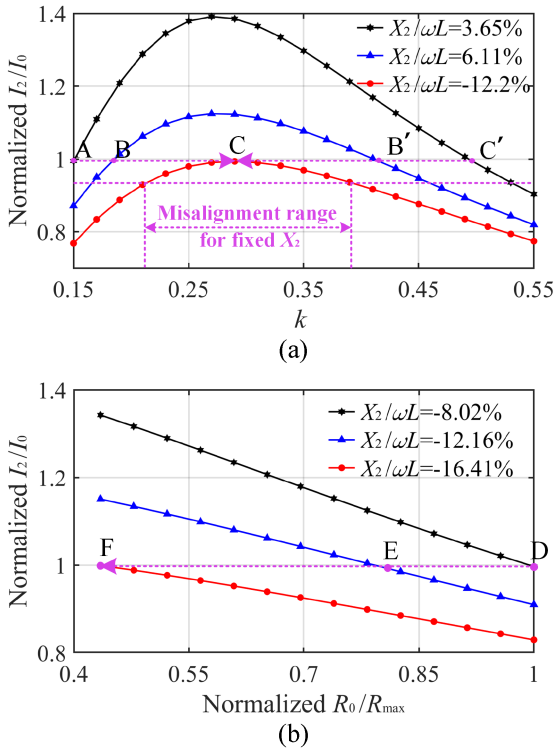

Fig. 3. Simulation results. (a) k versus I_0. (b) R_0 versus I_0.

higher power density and operating efficiency, the required adjustment range of VI should be as small as possible.

Therefore, the next section will give a detailed introduction to the parameter optimization process.

III. Design Procedure of the System

A. Design Considerations

In this section, a detailed design case of an IPT system with improved misalignment tolerance is proposed. The coupling coefficient ranges [$k_{\min}$, $k_{\max}$] and the load R_e ranges [$R_{\min}$, $R_{\max}$].

Once a working condition with a combination of parameters k and R_e is determined, the corresponding value of X_2 is a function of U_1 and X_1. Theoretically, there are numerous combinations for the two parameters to realize the required work. Moreover, in order for ZVS conditions to reduce power loss [23], a restriction for X_2 must be introduced, which is also in association with U_1 and X_1. Therefore, it is necessary to optimize the value of U_1 and compensation capacitor C_p.

B. Parameter Design

According to (9), the equation can be transformed as a function of X_2

$$F(X_2) = \frac{X_1^2 X_2^2}{\omega^2 k^2 L^2} - 2X_1X_2 + \frac{X_1^2 R_e^2}{\omega^2 k^2 L^2} + \omega^2 k^2 L^2 - \left(\frac{V_1}{I_0}\right)^2 \tag{10}$$

where I_0 is the required output current, the solution of equation $F(X_2) = 0$ is

$$X_{2\pm} = \frac{\omega^2 k^2 L^2}{X_1} \pm \frac{\omega k L}{X_1}\sqrt{\frac{V_1^2}{I_0^2} - \frac{X_1^2 R_e^2}{\omega^2 k^2 L^2}}. \tag{11}$$

Then, we can transform the problem into $\forall k \in [k_{\min}, k_{\max}], R_e \in [R_{\min}, R_{\max}]$, there always be a real solution of X_2 for the function. That is, the polynomial Δ in the root must be positive. Therefore, the minimum value of Δ should be larger than 0. And the $\Delta_{\min}$ is acquired with the minimum coupling coefficient $k_{\min}$ and the maximum value of load $R_{\max}$. Therefore, the following equation needs to be satisfied:

$$\begin{aligned} &\frac{X_1^2 R_{\max}^2}{\omega^2 L^2 k_{\min}^2} - \left(\frac{V_1}{I_0}\right)^2 \le 0 \\ &\Rightarrow |X_1| \le \frac{\omega L k_{\min} V_1}{R_{\max} I_0}. \end{aligned} \tag{12}$$

Then, we can assume that

$$|X_1| = \alpha \frac{\omega L k_{\min} V_1}{R_{\max} I_0}, \ (0 < \alpha \le 1). \tag{13}$$

In addition, to ensure an inductive input impedance, the phase angle and rms value of I_1 are deduced based on (7) and (11) as follows:

$$\tan\theta = \frac{X_2}{R_e} - \frac{(R_e^2 + X_2^2)X_1}{\omega^2 k^2 L^2 R_e} \tag{14}$$

$$|I_1| = \frac{I_0\sqrt{R_e^2 + X_2^2}}{\omega k L}. \tag{15}$$

Substitute (11) into (14), then the following equation can be obtained:

$$\tan\theta_{\pm} = \frac{1}{X_1 R_e}\left(-\left(\frac{V_1}{I_0}\right)^2 \mp \omega k L\sqrt{\left(\frac{V_1}{I_0}\right)^2 - \frac{X_1^2 R_e^2}{\omega^2 k^2 L^2}}\right). \tag{16}$$

To obtain an inductive input impedance, tanθ must be smaller than 0. According to (11) and (16), since the values of X_2 and X_1 can be positive or negative, there will be four cases that may satisfy the requirements. Next, the four cases are analyzed in detail to get the optimized situation.

Case A. $X_1 > 0, \theta_-$: For this case, the tangent value of θ_- and the corresponding X_2 are expressed as follows:

$$\tan\theta_- = \frac{1}{X_1 R_e}\left(-\left(\frac{V_1}{I_0}\right)^2 + \omega k L\sqrt{\left(\frac{V_1}{I_0}\right)^2 - \frac{X_1^2 R_e^2}{\omega^2 k^2 L^2}}\right) \tag{17}$$

$$X_{2-} = \frac{\omega^2 k^2 L^2}{X_1} - \frac{\omega k L}{X_1}\sqrt{\frac{V_1^2}{I_0^2} - \frac{X_1^2 R_e^2}{\omega^2 k^2 L^2}} \propto f(R, \mathrm{k}). \tag{18}$$

Based on (17), the condition of θ being negative can be further simplified as

$$\begin{aligned} &\left(-\left(\frac{V_1}{I_0}\right)^2 + \omega k L\sqrt{\left(\frac{V_1}{I_0}\right)^2 - \frac{X_1^2 R_e^2}{\omega^2 k^2 L^2}}\right)_{\max} \le 0 \\ &\Rightarrow \frac{V_1}{I_0} \ge \omega k_{\max} L\sqrt{1 - \frac{\alpha^2}{\beta^2\gamma^2}}. \end{aligned} \tag{19}$$

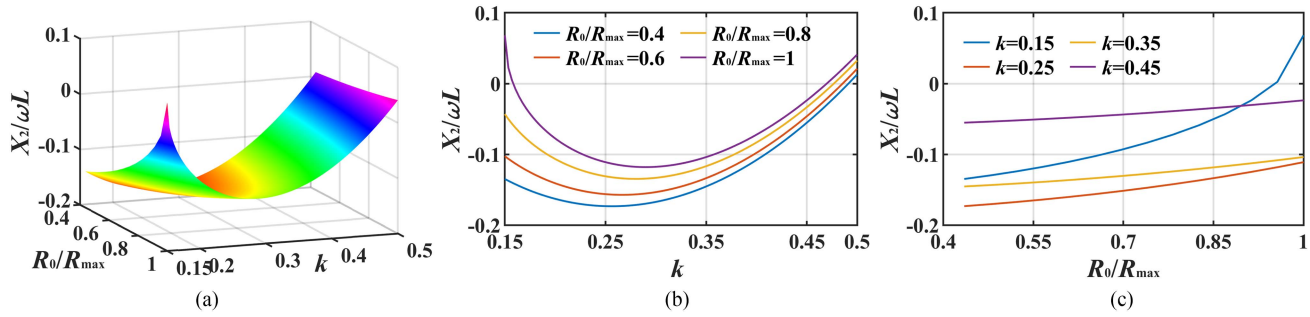

Fig. 4. *Case A:* required value of X_2 versus R_0 and k. (a) Three dimension. (b) X_2 versus k. (c) X_2 versus R_0.

Here, β and γ are given indexes, followed as

$$\beta = \frac{M_{\max}}{M_{\min}}, \gamma = \frac{R_{\max}}{R_{\min}}. \tag{20}$$

According to (19), a smaller α requires a higher input voltage to cover the whole region for ZVS. Therefore, $\alpha = 1$ is chosen here to lower the voltage stress. Then, (19) can be transformed into (21), and X_1 in this case is expressed by (22)

$$\frac{V_1}{I_0} = \omega k_{\max} L \sqrt{1 - \frac{1}{\beta^2 \gamma^2}} \tag{21}$$

$$X_1 = \frac{\omega L k_{\min} V_1}{R_{\max} I_0}. \tag{22}$$

Having obtained the design principle of V_1, the next step is to figure out the maximum and minimum value of X_2. It is a function of k and R_e (R_0) as $f(R, k)$. Owing to the fact that X_2 versus R_0 is a monotonic increasing function, we just have to consider k versus X_2. When k ranges from $k_{\min}$ to $k_{\max}$ with a fixed load R_0, X_2 will decrease initially, followed by an increase. Therefore, there are three states of the selected range of k, as shown in Fig. 4(b). With $k_{\min}$ and $k_{\max}$ both in *Region 1* or *2* or across the two regions, here the k_{op} may be out of the range. Then, the required maximum and minimum value of X_2 is expressed as follows:

$$X_{2\_\max} = \max\left\{f\left(R_{\max}, k_{\max}\right), f\left(R_{\max}, k_{\min}\right)\right\} \tag{23}$$

$$X_{2\_\min} = \begin{cases} f\left(R_{\min}, k_{op}\right), & k_{\min} < k_{op} < k_{\max} \\ \min\left\{f\left(R_{\min}, k_{\min}\right), f\left(R_{\min}, k_{\max}\right)\right\}, & k_{\text{op}} \geq k_{\max}, k_{\text{op}} \leq k_{\min}. \end{cases} \tag{24}$$

By applying (21) and (22) to (23), we have

$$f\left(R_{\max}, k_{\min}\right) = \frac{\omega^2 k_{\min}^2 L^2}{X_1} \tag{25}$$

$$f\left(R_{\max}, k_{\max}\right) = \frac{\omega^2 L^2 k_{\max}^2}{X_1} - \frac{\omega L k_{\max} V_1}{X_1 I_0} \sqrt{\left(1 - \frac{1}{\beta^2}\right)}. \tag{26}$$

Then, we have

$$\begin{aligned} &f\left(R_{\max}, k_{\min}\right) - f\left(R_{\max}, k_{\max}\right) \\ &= \frac{\omega^2 L^2 k_{\min}^2}{X_1} \sqrt{\beta^2 - 1} \left(\sqrt{\beta^2 - \frac{1}{\gamma^2}} - \sqrt{\beta^2 - 1}\right) > 0. \end{aligned} \tag{27}$$

Therefore, the required maximum value of X_2 in *Case A* can be got with $R_{\max}$ and $k_{\min}$ as (25).

Substituting (21) and (22) into (25), then (25) can be further expressed as

$$X_{2\_\max} = \frac{\omega^2 L^2 k_{\min}^2}{X_1} = \frac{R_{\max}}{\sqrt{\beta^2 - \frac{1}{\gamma^2}}}. \tag{28}$$

Based on (18), the partial derivative of k_{op} with k is used to identify k_{op} as expressed in (31)

$$\frac{\partial f}{\partial k} = \frac{2\omega^2 k L}{X_1} - \frac{\omega^2 V_1^2}{\sqrt{\omega^2 k^2 L^2 V_1^2 I_0^2 X_1^2 - R_e^2 I_0^4 X_1^4}}. \tag{29}$$

Then, k_{op} can be expressed as

$$k_{\text{op}} = \frac{1}{\omega L} \sqrt{\frac{V_1^2}{4 I_0^2} + \frac{R_e^2 X_1^2 I_0^2}{V_1^2}}. \tag{30}$$

By applying (21) and (22) to (30), k_{op} can also be expressed as

$$\begin{aligned} k_{op} &= \frac{1}{\omega \sqrt{L_1 L_2}} \sqrt{\frac{1}{4} \omega^2 L^2 k_{\max}^2 \left(1 - \frac{1}{\beta^2 \gamma^2}\right) + \frac{\omega^2 L^2 k_{\min}^2}{\gamma^2}} \\ &= k_{\min} \sqrt{\frac{\beta^2}{4} + \frac{3}{4\gamma^2}} > k_{\min} \\ &= k_{\max} \sqrt{\frac{1}{4} + \frac{3}{4\beta^2 \gamma^2}} < k_{\max}. \end{aligned} \tag{31}$$

It is obvious that k_{op} is among the value of $k_{\min}$ and $k_{\max}$. So we have

$$\begin{aligned} X_{2\_\min} &= f\left(R_{\min}, k_{\text{op}}\right) \\ &= \frac{R_{\min}}{\sqrt{\beta^2 \gamma^2 - 1}} - \frac{R_{\min}}{4} \sqrt{\beta^2 \gamma^2 - 1}. \end{aligned} \tag{32}$$

Case B. $X_1 > 0$, $\boldsymbol{\theta_+}$*:* For this case, the tangent value of θ_+ is expressed as follows, which is negative regardless of variations of parameters:

$$X_{2+} = \frac{\omega^2 k^2 L^2}{X_1} + \frac{\omega k L}{X_1} \sqrt{\frac{V_1^2}{I_0^2} - \frac{X_1^2 R_e^2}{\omega^2 k^2 L^2}} \propto f(R, \mathrm{k}) \tag{33}$$

$$\tan\theta_+ = \frac{1}{X_1 R_e}\left(-\left(\frac{V_1}{I_0}\right)^2 - \omega k L\sqrt{\left(\frac{V_1}{I_0}\right)^2 - \frac{X_1^2 R_e^2}{\omega^2 k^2 L^2}}\right). \tag{34}$$

A similar method is applied as above. However, X_2 versus R_0 here is a monotonic decreasing function. X_2 versus k here is a monotonic increasing function. Therefore, the maximum and minimum value of X_2 is relatively easy to obtain as

$$X_{2\_\max} = \frac{\omega L k_{\min} R_{\max} I_0}{\alpha V_1}\beta^2 + \frac{R_{\max}}{\alpha}\beta\sqrt{1-\frac{\alpha^2}{\beta^2\gamma^2}} \tag{35}$$

$$X_{2\_\min} = \frac{\omega L k_{\min} R_{\max} I_0}{\alpha V_1} + \frac{R_{\max}}{\alpha}\sqrt{1-\alpha^2}. \tag{36}$$

For this case, the value of X_2 is always positive. Since a larger V_1 and α lower the value of X_2. Correspondingly, the rms value of I_1 can be lower according to (15). Therefore, $\alpha = 1$ and (21) are also adopted here to give a comparison with *Case A*. Then, we have

$$X_{2\_\max} = \frac{\beta^2\gamma R_{\max}}{\sqrt{\beta^2\gamma^2-1}} + R_{\min}\sqrt{\beta^2\gamma^2-1} \tag{37}$$

$$X_{2\_\min} = \frac{R_{\max}}{\sqrt{\beta^2-\frac{1}{\gamma^2}}}. \tag{38}$$

For *Case B*, the required value of X_2 is much larger than *Case A*, which is difficult to design such a VI, and the power density will decrease significantly. Moreover, the increment of I_1 will decrease the total efficiency of the system.

Case C. $X_1 < 0, \theta_-$*:* Obviously, the tangent value and X_2 are the same as (17) and (18), and the difference is just the sign of X_1. The judgment condition of θ being negative is shown as

$$\begin{aligned}&\left(-\left(\frac{V_1}{I_0}\right)^2 + \omega k L\sqrt{\left(\frac{V_1}{I_0}\right)^2 - \frac{X_1^2 R_e^2}{\omega^2 k^2 L^2}}\right)_{\min} \geq 0\\ &\Rightarrow \omega L k_{\min}\sqrt{1-\alpha^2} \geq \frac{V_1}{I_0}.\end{aligned} \tag{39}$$

Here, the equal sign is applied to decrease the value of input current. Substituting (13) and (39) into (31), we have

$$k_{\text{op}} = k_{\min}\sqrt{\frac{1}{4}+\frac{\alpha^2}{\gamma^2}-\frac{\alpha^2}{4}} < k_{\min}. \tag{40}$$

In *Case C*, the value of k_{op} is smaller than $k_{\min}$. So X_2 here versus R_0 here will decrease when k increases. Because of the sign change of X_1, X_2 versus R_0 here becomes a monotonic decreasing function Then, we have

$$X_{2\_\max} = f(R_{\min}, k_{\min}) = \frac{R_{\max}}{\alpha\sqrt{1-\alpha^2}} + R_{\min}\sqrt{\frac{\gamma^2}{\alpha^2}-1} \tag{41}$$

$$X_{2\_\min} = f(R_{\max}, k_{\max}) = \frac{R_{\max}\beta^2}{\alpha\sqrt{1-\alpha^2}} + R_{\max}\sqrt{\frac{\beta^2}{\alpha^2}-1}. \tag{42}$$

Case D. $X_1 < 0$, $\boldsymbol{\theta_+}$*:* Obviously, this case should be rejected since the tangent value is always positive.

TABLE I
SYSTEM PARAMETERS OF THE REQUIRED OPERATION

Indexes	Constraints
Coil size (mm)	300 × 300
Output current change rates, I (A)	6.5 ± 0.3 (5%)
Operating frequency (kHz)	85
Load resistance (Ω)	10–23
Variation of coupling coefficient	0.15–0.5

TABLE II
PARAMETERS OF THE DESIGNED PROTOTYPE

Parameters	Value
Input voltage V_1 (V)	320
Operating frequency f (kHz)	85
Output current I_0 (A)	6.5
Load resistance (Ω)	10–23
Inductance of primary coil L1 (μH)	159
Compensation capacitor C1 (nF)	32.2
Inductance of secondary coil L2 (μH)	151
Compensation capacitor C2 (nF)	17.5
VI core shape	EE70B
VI Air gap δ (mm)	2
VI main winding turns N_{ac}	10
Auxiliary winding turns N_{dc}	30
VI total volume (mm^3)	70.7 × 66.4 × 30.5
Inductance of VI (μH)	23–60

To summarize, the design process is summarized as follows:

Step 1: According to the maximum dimension of the coils, the self-inductance is acquired based on simulation of Maxwell.
Step 2: According to (21), the value of input voltage V_1 can be obtained.
Step 3: According to (22), the primary compensation capacitor C_1 is determined.
Step 4: Calculate the required range of X_2.
Step 5: Properly adjust the value of C_2, so that the required VI can be well designed with a relatively small amplitude value of I_1 to reduce power loss.

By applying the parameters in Table I, the values of X_2 versus R_0 and k for different cases can be obtained as shown in Figs. 4–6. It is notable that *Case A* is suitable to be applied for design of the IPT system with the smallest variation of X_2. When R_0 is 10 Ω, X_2 varies from −26 to 5. The minimum value −26 is acquired when k is equal to about 0.25. The maximum value of X_2 is about 10, which is acquired when k is equal to 0.15 and R_0 is equal to 23 Ω.

Based on (6), (21), (22), (28), and (32), the final optimized system parameters are shown in Table II.

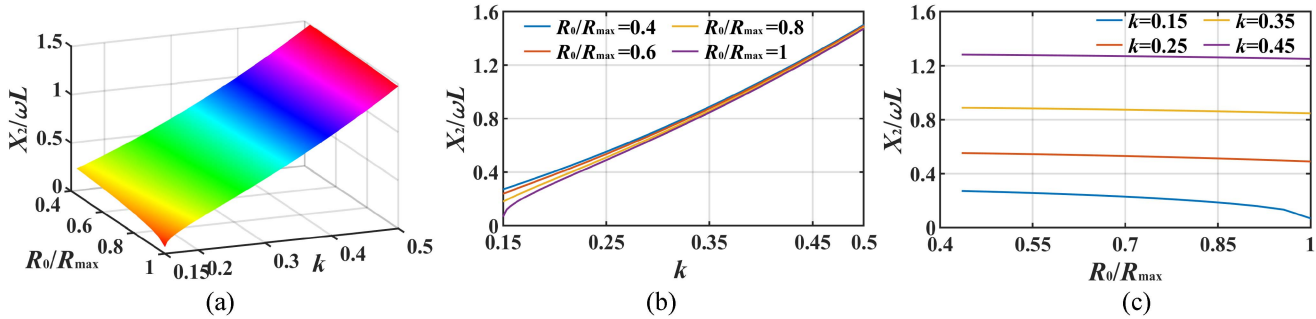

Fig. 5. *Case B:* required value of X_2 versus R_0 and k. (a) Three dimension. (b) X_2 versus k. (c) X_2 versus R_0.

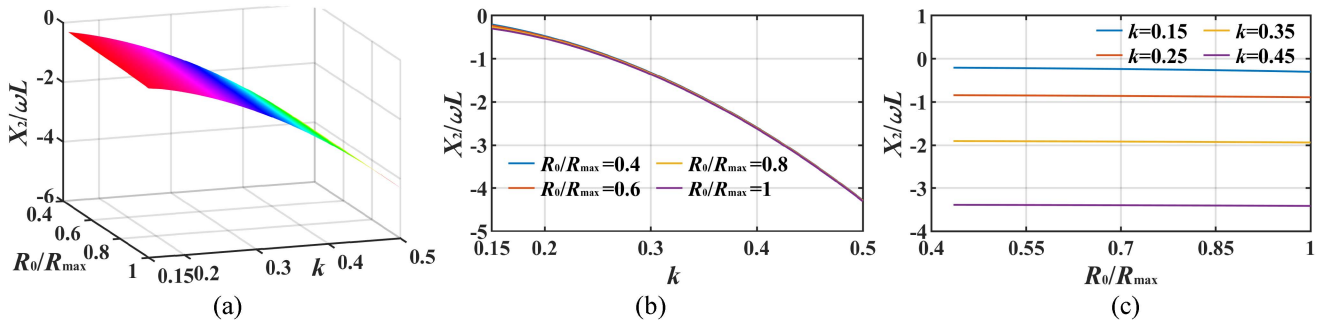

Fig. 6. *Case C:* required value of X_2 versus R_0 and k. (a) Three dimension. (b) X_2 versus k. (c) X_2 versus R_0.

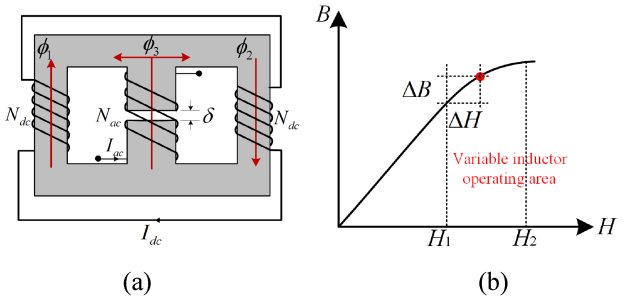

Fig. 7. Variable inductor. (a) Structure. (b) Hysteresis curve.

IV. Implementation of VI System

A. Design of VI

VI is based on the modulation of the permeability of its ferromagnetic core by a biased magnetic field produced by an auxiliary coil. The ac inductance $L_{\rm ac}$ is wound in the middle leg of the core, which contains an air gap to avoid magnetic saturation. Two identical control windings $L_{\rm bias}$ are placed in the outer legs. The control windings are serially connected in opposite polarity so as to generate reversed magnetic flux directions and cancel out the ac voltages induced by the center leg, as shown in Fig. 7. The basic idea is to control the main inductor $L_{\rm ac}$ by altering the outer arms' permeances. A dc current source circulating through $L_{\rm bias}$ can be adopted to modify the equivalent inductance $L_{\rm ac}$: the larger the dc current, the smaller the inductor. Based on the analysis in Section III, the required L_1 varies from 30 to 60 μH. With the help of simulation, the parameters of VI are designed with a total volume of 70.7 $\times$ 66.4 $\times$ 30.5 mm^3.

Characteristics of the VI are measured using an IM3536 LCR Meter. The maximum inductance is about 60 μH. The whole range versus dc current is shown in Fig. 8.

B. Adjustment Strategy of VI

According to (18), the regulation of the inductor seems to be complex because of the variation of k and R_0. The two parameters are difficult for identification. However, based on the analysis in Section III, we can also get that

$$I_2 \propto g\left(X_2\right) = \frac{U_1}{\sqrt{\omega^2 k^2 L^2 + \frac{X_1^2\left(R_e^2+X_2^2\right)}{\omega^2 k^2 L^2} - 2X_1X_2}} \tag{43}$$

$$X_2 = \frac{\omega^2 k^2 L^2}{X_1} - \frac{\omega k L}{X_1}\sqrt{\frac{V_1^2}{I_0^2} - \frac{X_1^2 R_e^2}{\omega^2 k^2 L^2}}. \tag{44}$$

Obviously, there is only one pole for the function (44), the value of which is

$$X_{2\_\rm pole} = \frac{\omega^2 k^2 L^2}{X_1} \tag{45}$$

where X_1 and ω are constant, and M_1 is variable. The minimum value of $X_{2\cdot\rm pole}$ is obtained when k equals $k_{\rm min}$. According to (28), the upper boundary of X_2 is equal to the minimum value of $X_{2\cdot\rm pole}$. Therefore, I_2 versus X_2 is a monotonic increasing function. The adjustment strategy of VI is monotonic.

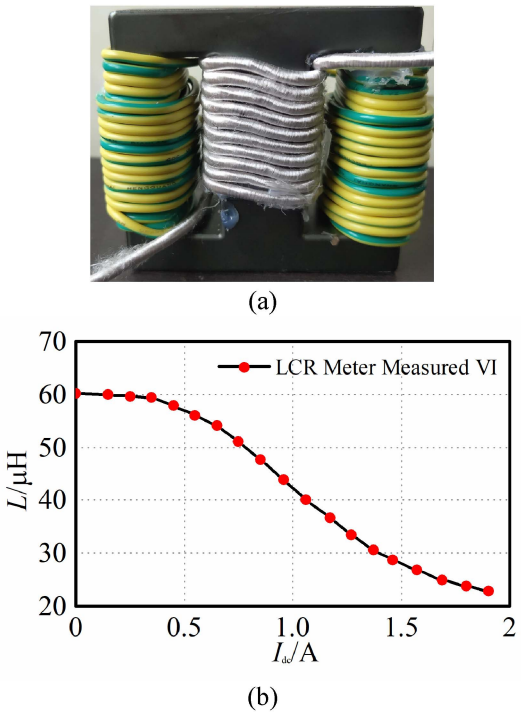

Fig. 8. (a) Constructed variable inductor. (b) LCR meter measurements.

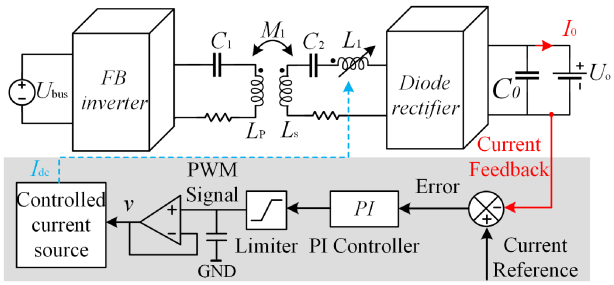

Fig. 9. Control strategy of the system.

C. Control Method

The control flowchart of the system is depicted in Fig. 9. Based on the analysis above, the output current I_2 versus X_2 is a monotonic increasing function regardless of variations of k and R_0. In addition, the smaller the control current i_{dc}, the larger the equivalent inductance L_{ac} (X_2). Therefore, if the measured output current is smaller than the rated current, it will cause a deviation Δi. Then, the value of i_{dc} will decrease to seek the required output current level. The PI controller will output a PWM duty cycle which can be transformed into the variation of v with an LPF. In order to improve the driving ability, a voltage controlled current source with a MOSFET is used. The gate voltage v is controlled by the PI controller to adjust the dc current.

V. Experimental Validation

A. Experiment Prototype Design

A prototype of 1-kW output power is built to verify the analysis, as shown in Fig. 10. The transmitter and receiver coil

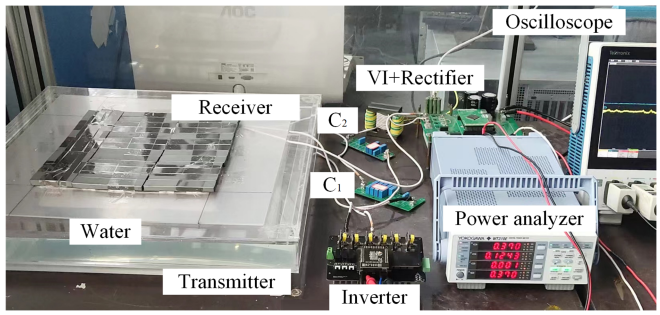

Fig. 10. Experimental setup of the IPT system.

size are both 300 × 300 mm with PC40 ferrite full coverage to reduce the emission. A diameter of 4-mm Litz-wire and a thickness of 5-mm ferrite are employed to fabricate the coils. The gap changes from 50 to 120 mm, which is full of salt water with a conductivity of 3 S/m.

On the primary side, a programmable dc source is applied for power supply. A full-bridge inverter is constructed using four silicon carbide MOSFETs (IMZ65R048M1) to convert the dc voltage to ac voltage. On the secondary side, the diodes for the full-bridge rectifier are IDW60C65D1XKSA1. An electronic load is used to take the place of battery for analysis. The equivalent load resistance can be continuously adjusted. In addition, a WT500 power analyzer is used to measure the efficiency. The controller is TMS320F280049. The coupling coefficient k of the coils is measured to be 0.5 in well-aligned condition, 0.15 in 140-mm horizontal misalignment, and 0.2 in 90-mm vertical misalignment.

B. Experimental Results

During experiments, the prototype is tested for various conditions of coupling coefficient k and load resistance R_0. The VI is regulated to achieve a CC output.

Fig. 11 shows the CC output characteristics of the charging system. Here a range covers the common charging voltage, 72 and 144 V for AUVs is employed. The rectifier input voltage and current are measured. It can be observed that the current keeps almost unchanged with an amplitude of 10.3 A as the load increases from 10 to 23 Ω.

The primary input voltage and current under the nominal load 23 Ω with the coupling coefficient k equals 0.5, 0.25, and 0.15 are provided in Fig. 12. When the coupling coefficient k becomes 0.15. the dc input voltage is still 320 V. For an SS-IPT system, the output current is reversely proportional to the coupling coefficient k. Fig. 12 shows that, for the misalignment working condition, the phase shift between input voltage and current is obvious. The reactive power is significant to keep the rated output power. At the well-aligned position, the input voltage and current are almost in phase, and the harmonics help the realization of ZVS as shown in Fig. 12(a). When the misalignment increases, the phase angle increases to around 67°, as shown in Fig. 12(c), ZVS can be realized in the whole range.

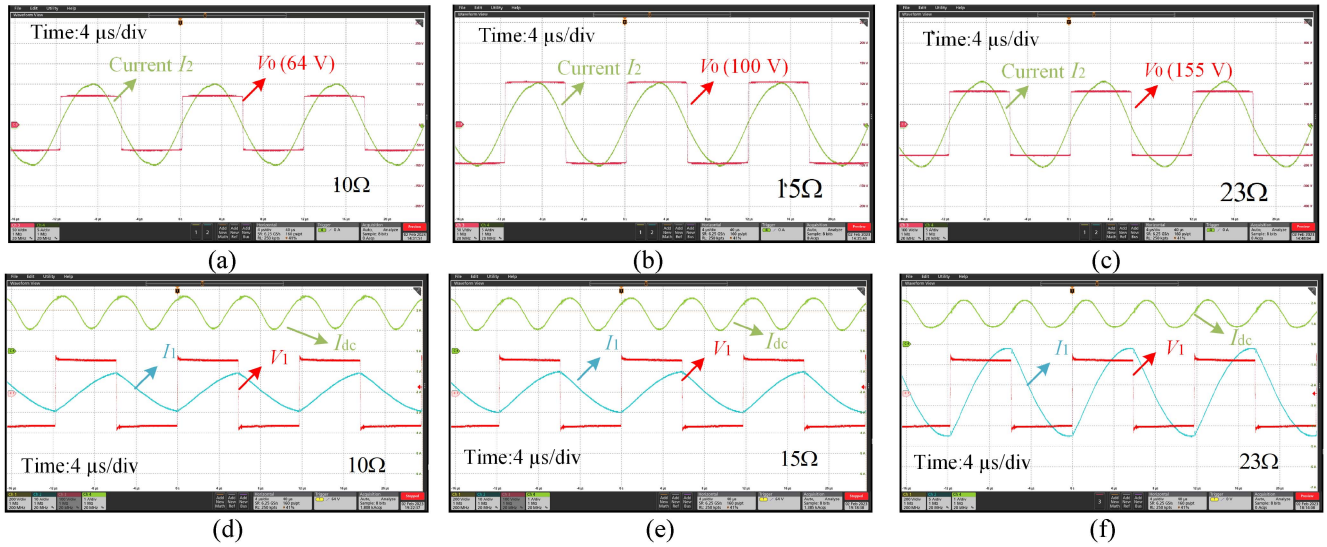

Fig. 11. CC verification under load variations. (a), (d) 10 Ω. (b), (e) 15 Ω. (c), (f) 23 Ω.

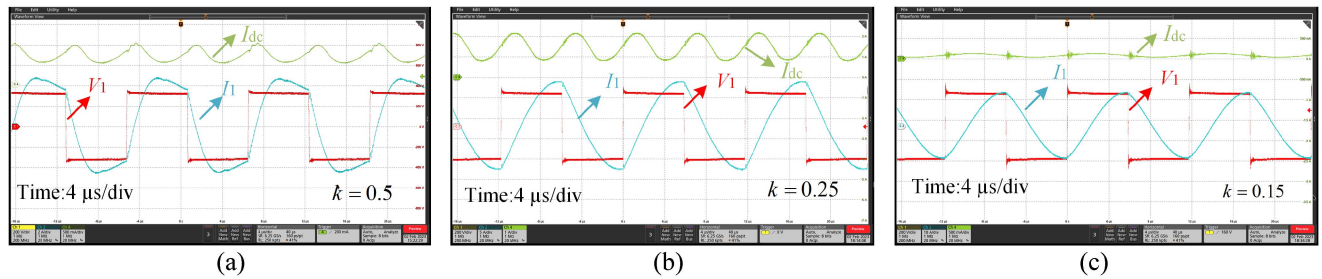

Fig. 12. Waveforms of input voltage and current and control DC current. (a) $k = 0.5$. (b) $k = 0.25$. (c) $k = 0.15$.

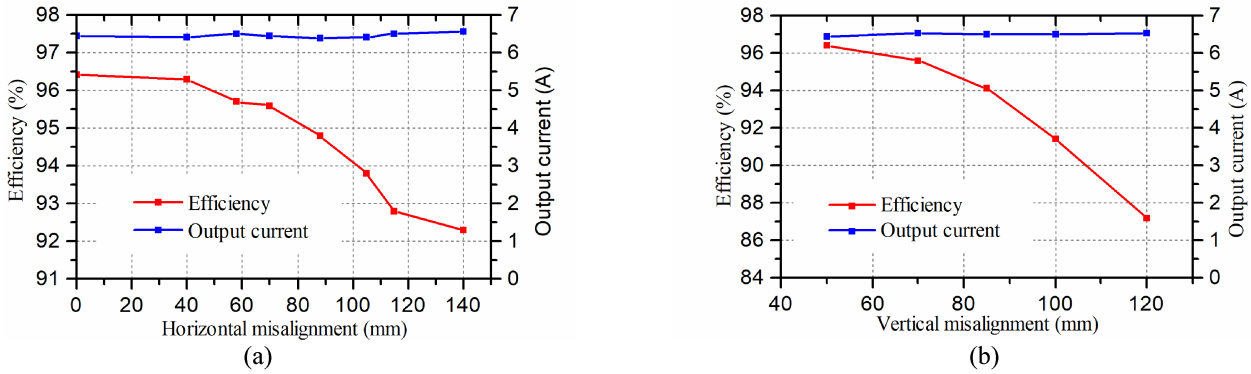

Fig. 13. RMS value of output current and efficiency versus misalignment. (a) Horizontal. (b) Vertical.

Fig. 13 verifies the misalignment tolerance of the proposed system. The experiments are carried out under X-axis misalignment varying from 0 to 140 mm and Z-axis misalignment varying from 0 to 70 mm, respectively. The output current and efficiency are measured. For Fig. 13(a), the gap is 50 mm. The output current stays stable to be around 6.5 A as misalignment increases from 0 to 140 mm, which proves the feasibility of the proposed system. The efficiency of the system drops from 96.1% to 92.3%. The 3.8% drop in efficiency is mainly due to the reactive power in misalignment condition. However, it is still relatively high in this high misalignment scenario.

Fig. 13(b) shows the experimental results in the case when vertical misalignment occurs with a gap of 120 mm. Due to the detuning of the compensation topology, the reactive power is still significant. The transfer current is constant with 96.1% to 87.8% efficiency as shown in Fig. 14. Compared to horizontal misalignment, the efficiency is lower for vertical misalignment. Two reasons contribute to the drop in efficiency. First, when

TABLE III
COMPARISON WITH VARIOUS METHODS

References	strategy	Misalignment tolerance (mm)	k variation	Power and efficiency	Components	Wireless communication
This article	Secondary VI[1]	***XY*: 0–140 (47%)** ***Z*: 50–120 (140%)**	**0.15–0.5**	1 kW **96.1%**	2 Coil + 2C + 1VI	**No**
[16]	Hybrid compensation[2]	*XY*: 0–70 (29%) *Z*: 55–100 (82%)	0.135–0.345	250 W 94.3%	4Coil + 6C	No
[27]	DC/DC converters[3]	*XY*: N/A *Z*: 25–45 (80%)	0.122–0.254	100 W 89.3%	2Coil + 2C + 2dc/dc	Required
[33]	Primary VLC[2]	*XY*: 0–200 (40%) *Z*: N/A	0.08–0.18	3.3 kW 87.5%	2Coil + 3C + 1L + 1VLC	No
[32]	Primary VI + DD coupler[1]	*XY*: 0–130 (22%) 0–310 (49%) *Z*: N/A	0.135–0.22	3.3 kW **96.1%**	2Coil + 2C + 1VI	Required
[28]	Active rectifier[3]	*XY*: 0–200 (33%) *Z*: 100–170 (70%)	0.24–0.45	3 kW 96%	2Coil + 2C	Required
[29]	Active rectifier[4]	*XY*: N/A *Z*: 125–190 (52%)	0.1–0.2	288 W 96.8%	2Coil + 2C	Required

* represents the complexity level of the system, [1] means the lowest level, and [4] means the highest level.

(a) (b)

Fig. 14. Power meter. (a) Well aligned. (b) 120-mm vertical misalignment.

the gap increases, the self-inductance $L_{1(2)}$ may decrease, the current I_1 increases with lower L_1 and L_2 as shown in (15). The increased current may cause additional loss in coils and the eddy current loss will also be larger. Second, the expansion of the gap further increases eddy current loss.

C. Comparison With Previous Literature

Various methods to improve the misalignment tolerance are introduced in Table III. Compared with the other literature, the significant advantage of the proposed method is higher misalignment tolerance with no wireless communication, which is suitable for underwater IPT systems.

The allowable coupling coefficient range $k_{\max}/k_{\min}$ of this article is the largest. That means the proposed method has a better anti-misaligment capability, especially in the z-direction. Based on the previous analysis, the proposed control method can also be applied to various magnetic couplers to further improve the misalignment tolerant.

This article aims to propose an IPT system design and operation method for CC output at any battery equivalent load resistance and misalignment in a specific charging scenario. In this article, both the coupling coefficient fluctuation and varying battery voltage are considered for parameter design of the whole system. At any condition among the specific charging area, the IPT system is designed to regulate the output current at a constant value. The significant advantage of the proposed method is higher anti-misalignment in both horizontal (47%) and vertical directions (140%). Further, only one controller is needed and the control does not rely on communication. In summary, the proposed system is suitable for applications underwater.

VI. CONCLUSION

In this article, a design methodology of the IPT system with VI to maintain CC output within a wide range of misalignment and load resistance has been proposed. The principle of the proposed method is analyzed based on the mathematical model. For various requirements of k and R_0 variation, the system can be designed flexibly with a quite simple control strategy without a communication link. Finally, a prototype with a 1-kW output power is built to verify the method. The experimental results show that the output current is almost constant when k varies from 0.15 to 0.5 in XY- and Z- directions and output voltage from 64 to 150 V. When the output power is 1 kW, the system efficiency exceeds 87%, the horizontal misalignment range is 47%, and the vertical misalignment range is 140%, which is superior to the commonly used methods. The proposed WPT system suits applications for AUVs, in which stable wireless communication is difficult, and a high vertical misalignment may occur during charging.

REFERENCES

[1] S. Hui and W. Ho, "A new generation of universal contactless battery charging platform for portable consumer electronic equipment," *IEEE Trans. Power Electron.*, vol. 20, no. 3, pp. 620–627, May 2005.
[2] S. Y. R. Hui, W. Zhong, and C. K. Lee, "A critical review of recent progress in mid-range wireless power transfer," *IEEE Trans. Power Electron.*, vol. 29, no. 9, pp. 4500–4511, Sep. 2014.
[3] S. Li and C. C. Mi, "Wireless power transfer for electric vehicle applications," *IEEE Trans. Emerg. Sel. Topics Power Electron.*, vol. 3, no. 1, pp. 4–17, Mar. 2015.
[4] C. R. Teeneti, T. T. Truscott, D. N. Beal, and Z. Pantic, "Review of wireless charging systems for autonomous underwater vehicles," *IEEE J. Ocean. Eng.*, vol. 46, no. 1, pp. 68–87, Jan. 2021.

[5] M. Lin, D. Li, and C. Yang, "Design of an ICPT system for battery charging applied to underwater docking systems," *Ocean. Eng.*, vol. 145, pp. 373–381, 2017.
[6] S. Raabe and G. A. Covic, "Practical design considerations for contactless power transfer quadrature pick-ups," *IEEE Trans. Ind. Electron.*, vol. 60, no. 1, pp. 400–409, Jan. 2013.
[7] W. Zhao, X. Qu, J. Lian, and C. K. Tse, "A family of hybrid IPT couplers with high tolerance to pad misalignment," *IEEE Trans. Power Electron.*, vol. 37, no. 3, pp. 3617–3625, Mar. 2022.
[8] Z. Yan, M. Wu, C. Zhao, Q. Hu, and L. Wang, "Free-rotation wireless power transfer system based on composite anti-misalignment method for AUVs," *IEEE Trans. Power Electron.*, vol. 38, no. 4, pp. 4262–4266, Apr. 2023.
[9] H. P. Zhang, C. H. T. Lee, X. Xu, X. Wei, and J. Wang, "Comparative analysis and optimization of dynamic charging coils for roadway-powered electric vehicles," *IEEE Trans. Magn.*, vol. 53, no. 11, Nov. 2017, Art. no. 9402106.
[10] M. S. Zhang, O. C. Onar, Q. Yang, and C. Cai, "A field enhancement integration design featuring misalignment tolerance for wireless EV charging using LCL topology," *IEEE Trans. Power Electron.*, vol. 36, no. 4, pp. 3852–3867, Apr. 2021.
[11] Z. Yuan, M. Saeedifard, C. Cai, Q. Yang, and H. Lin, "A misalignment tolerant design for a dual-coupled LCC-S-compensated WPT system with load-independent CC output," *IEEE Trans. Power Electron.*, vol. 37, no. 6, pp. 7480–7492, Jun. 2022.
[12] Y. Chen, R. Mai, Y. Zhang, M. Li, and Z. He, "Improving misalignment tolerance for IPT system using a third-coil," *IEEE Trans. Power Electron.*, vol. 34, no. 4, pp. 3009–3013, Apr. 2019.
[13] J. Hou, Q. Chen, Z. Zhang, S. C. Wong, and C. K. Tse, "Analysis of output current characteristics for higher-order primary compensation in inductive power transfer systems," *IEEE Trans. Power Electron.*, vol. 33, no. 8, pp. 6807–6821, Aug. 2018.
[14] J. Mai, Y. Wang, Y. Yao, and D. Xu, "Analysis and design of high misalignment tolerant compensation topologies with constant-current or constant-voltage output for IPT systems," *IEEE Trans. Power Electron.*, vol. 36, no. 3, pp. 2685–2695, Mar. 2021.
[15] Y. Chen, B. Yang, Z. Kou, Z. He, G. Cao, and R. Mai, "Hybrid and reconfigurable IPT systems with high-misalignment tolerance for constant current and constant voltage battery charging," *IEEE Trans. Power Electron.*, vol. 33, no. 10, pp. 8259–8269, Oct. 2018.
[16] G. Ke, Q. Chen, L. Xu, X. Ren, and Z. Zhang, "Analysis and optimization of a double-sided S-LCC hybrid converter for high misalignment tolerance," *IEEE Trans. Ind Electron.*, vol. 68, no. 6, pp. 4870–4881, Jun. 2021.
[17] L. Zhao, D. J. Thrimawithana, U. K. Madawala, A. P. Hu, and C. C. Mi, "A misalignment-tolerant series-hybrid wireless EV charging system with integrated magnetics," *IEEE Trans. Power Electron.*, vol. 34, no. 2, pp. 1276–1285, Feb. 2019.
[18] Z. Liu, M. Su, Q. Zhu, L. Zhao, and A. P. Hu, "A dual frequency tuning method for improved coupling tolerance of wireless power transfer system," *IEEE Trans. Power Electron.*, vol. 36, no. 7, pp. 7360–7365, Jul. 2021.
[19] L. Zhao, D. J. Thrimawithana, and U. K. Madawala, "Hybrid bidirectional wireless EV charging system tolerant to pad misalignment," *IEEE Trans. Ind. Electron.*, vol. 64, no. 9, pp. 7079–7086, Sep. 2017.
[20] Y. Yao, Y. Wang, X. Liu, K. Lu, and D. Xu, "Analysis and design of an S/SP compensated IPT system to minimize output voltage fluctuation versus coupling coefficient and load variation," *IEEE Trans. Veh. Technol.*, vol. 67, no. 10, pp. 9262–9272, Oct. 2018.
[21] J. Yang, X. Zhang, K. Zhang, X. Cui, C. Jiao, and X. Yang, "An LCC-SP compensated inductive power transfer system and design considerations for enhancing misalignment tolerance," *IEEE Access*, vol. 8, pp. 193285–193296, 2020.
[22] A. Ramezani and M. Narimani, "Optimized electric vehicle wireless chargers with reduced output voltage sensitivity to misalignment," *IEEE J. Emerg. Sel Topics Power Electron.*, vol. 8, no. 4, pp. 3569–3581, Dec. 2020.
[23] M. Kim, D.-M. Joo, and B. K. Lee, "Design and control of inductive power transfer system for electric vehicles considering wide variation of output voltage and coupling coefficient," *IEEE Trans. Power Electron.*, vol. 34, no. 2, pp. 1197–1208, Feb. 2019.
[24] J. Li, X. Zhang, and X. Tong, "Research and design of misalignment-tolerant LCC-LCC compensated IPT system with constant-current and constant-voltage output," *IEEE Trans. Power Electron.*, vol. 38, no. 1, pp. 1301–1313, Jan. 2023.
[25] N. Liu and T. G. Habetler, "Design of a universal inductive charger for multiple electric vehicle models," *IEEE Trans. Power Electron.*, vol. 30, no. 11, pp. 6378–6390, Nov. 2015.
[26] H. Zhu, B. Zhang, and L. Wu, "Output power stabilization for wireless power transfer system employing primary-side-only control," *IEEE Access*, vol. 8, pp. 63735–63747, 2020.
[27] Z. Huang, S.-C. Wong, and C. K. Tse, "Control design for optimizing efficiency in inductive power transfer systems," *IEEE Trans. Power Electron.*, vol. 33, no. 5, pp. 4523–4534, May 2018.
[28] T. Diekhans and R. W. D. Doncker, "A dual-side controlled inductive power transfer system optimized for large coupling factor variations and partial load," *IEEE Trans. Power Electron.*, vol. 30, no. 11, pp. 6320–6328, Nov. 2015.
[29] Y. Jiang, L. Wang, J. Fang, C. Zhao, K. Wang, and Y. Wang, "A joint control with variable ZVS angles for dynamic efficiency optimization in wireless power transfer system," *IEEE Trans. Power Electron.*, vol. 35, no. 10, pp. 11064–11081, Oct. 2020.
[30] Y. Liu, U. K. Madawala, R. Mai, and Z. He, "Zero-phase-angle controlled bidirectional wireless EV charging systems for large coil misalignments," *IEEE Trans. Power Electron.*, vol. 35, no. 5, pp. 5343–5353, May 2020.
[31] J. Zhang, J. Zhao, Y. Zhang, and F. Deng, "A wireless power transfer system with dual switch-controlled capacitors for efficiency optimization," *IEEE Trans. Power Electron.*, vol. 35, no. 6, pp. 6091–6101, Jun. 2020.
[32] Z. Zhang, F. Zhu, D. Xu, P. T. Krein, and H. Ma, "An integrated inductive power transfer system design with a variable inductor for misalignment tolerance and battery charging applications," *IEEE Trans. Power Electron.*, vol. 35, no. 11, pp. 11544–11556, Nov. 2020.
[33] K. Song, Y. Lan, R. Wei, G. Yang, F. Yang, and Y. Li, "A control strategy for wireless EV charging system to improve weak coupling output based on variable inductor and capacitor," *IEEE Trans. Power Electron.*, vol. 37, no. 10, pp. 12853–12864, Oct. 2022.
[34] Y. Chen, S. He, B. Yang, S. Chen, Z. He, and R. Mai, "Reconfigurable rectifier-based detuned series-series compensated IPT system for anti-misalignment and efficiency improvement," *IEEE Trans. Power Electron.*, vol. 38, no. 2, pp. 2720–2729, Feb. 2023.

Jia Li received the B.S. degree in mechanical engineering from the Shanghai Jiao Tong University, Shanghai, China, in 2020. He is currently working toward the Ph.D. degree in mechanical engineering with the Shanghai Jiao Tong University, Shanghai, China.

His research interests include wireless power transfer and its application in autonomous underwater vehicles, and power system stability and control.

Chong Zhu (Member, IEEE) received the B.S. degree in electrical engineering from the China University of Mining and Technology, Xuzhou, China, in 2010, and the Ph.D. degree in electrical engineering from the Zhejiang University, Hangzhou, China, in 2016.

He was a Postdoctoral Researcher with the San Diego State University, San Diego, CA, USA, from 2017 to 2019. He is currently an Assistant Professor with the School of Mechanical Engineering, Shanghai Jiao Tong University, Shanghai, China. His research interests include battery thermal management, and design and control of power converters applied in electric vehicles.

Jixie Xie received the B.S. degree in energy and power engineering from the Southeast University, Nanjing, China, in 2017, and the M.Sc. degree in materials for energy and environment from the University College London, London, U.K., in 2018. He is currently working toward the Ph.D. degree in mechanical engineering with the Shanghai Jiao Tong University, Shanghai, China.

His research interests include wireless power transfer, magnetic shielding design, and resonant couplers optimization in autonomous underwater vehicles.

Fei Lu (Member, IEEE) received the B.S. and M.S. degrees in electrical engineering from the Harbin Institute of Technology, Harbin, China, in 2010 and 2012, respectively, and the Ph.D. degree in electrical engineering from the University of Michigan, Ann Arbor, MI, USA, in 2017.

He is currently an Assistant Professor with the Department of Electrical and Computer Engineering, Drexel University, Philadelphia, PA, USA. His research interests include power electronics and the application of electric vehicle charging.

Xi Zhang (Senior Member, IEEE) received the B.Sc. degree in applied mathematics and the B.E. degree in information and control engineering from the Shanghai Jiao Tong University (SJTU), Shanghai, China, in 2002, and the M.E. and Ph.D. degrees in power electronics and electric power drive from the SJTU, in 2004 and 2007, respectively.

From 2007 to 2009, he held a Postdoctoral position with the Department of Electrical and Computer Engineering, University of Michigan at Dearborn, Dearborn, MI, USA. He is currently a Professor with the Institute of Automotive Engineering and National Engineering Laboratory for Automotive Electronics and Control Technology, SJTU. His research interests include wireless charging, power management strategies, power electronics devices, and motor control systems of electric vehicle (EV)/hybrid EV.